Is there a brain area dedicated to socially guided spatial attention?

Marius Görner[1,2,3,*], Peter W Dicke[1], and Peter Thier[1,4,*]

[1] Hertie Institute for Clinical Brain Research, Thier Lab, Tübingen, Germany

[2] GTC of Neuroscience, Tübingen, Germany

[3] IMPRS for Cognitive and Systems Neuroscience, Tübingen, Germany

[4] Werner Reichardt Centre for Integrative Neuroscience, Tübingen Germany

[*] Corresponding authors: Peter Thier (thier@uni-tuebingen.de), Marius Görner (mariusgoerner@gmail.com)

Abstract

Apart from language, our gaze is arguably the most important means of communication. Where we look lets others know what we are interested in and allows them to join our focus of attention. In several studies our group investigated the neuronal basis of gaze following behavior in humans and macaques and described the *Gaze following patch* in the posterior temporal cortex as being of central importance for this function. To our knowledge, this makes it the most promising candidate for Simon Baron-Cohen's *Eye-Direction-Detector*, an integral part of his influential *Mindreading System.* With the latter, Baron-Cohen proposed a network of *domain-specific* neurocognitive modules that are necessary to establish a *Theory of Mind* - the attribution of mental states to others. The tenet of domain-specificity requires that the EDD processes only and exclusively eye-like stimuli with their typical contrast and movement properties. In the present fMRI study, we aim to critically test if the GFP fulfills this criterion. Specifically, we will test if it is equivalent to or different from the visual motion processing areas located in the same part of the brain. Since our experiments capture the full-behavioral relevance of gaze-following behavior and are specifically designed to reveal an EED our results will provide strong support or rejection of a central property Baron-Cohen's Mindreading-System – *domain specificity*.

Introduction

The direction of our gaze plays a fundamental role when we interact with a fellow human. Just by observing the other person's gaze during a conversation, we can often tell if interest is waning or growing. We can also use our own gaze to influence the other and to establish *joint attention,* an important precursor to a *Theory of Mind* (ToM). The latter concept captures our ability to attribute beliefs and intentions to others, basis of predicting behavior and necessary to optimally shape our own. With his *Mindreading System*, Simon Baron-Cohen suggested a neurocognitive system within which 4 *domain-specific* modules work together to enable the very behavior. In this, the *Eye Direction Detector* (EDD) is the node that contributes the information on gaze-direction which is integrated with information from an *Intentionality Detector* (ID) to form the *Shared Attention Mechanism* (SAM). Finally, the latter merges into the *Theory of Mind Mechanism* [1,2]. His understanding of modularity is based on Fodor proposals [3] which imply, among other things, that the EDD corresponds to a dedicated neural architecture that only and exclusively processes eye-like stimuli with their typical contrast and motion properties. Baron-Cohen's concept appears to be as highly influential (~500 citations) as it may be controversial in the light of the debate about oversimplified structure-function associations (see for example [4] or [5]).

However, given the ecological importance of judging gaze directions – whether for predator avoidance or social communication [6] – it seems conceivable that a specialized neural mechanism evolved to optimize processing in order to facilitate rapid behavioral responses. How fast you can detect a staring predator may decide upon life and death. Support for this idea is provided by behavioral studies showing that responses to gaze stimuli in both humans and macaques appear to be reflex like, i.e. they are fast and cannot be suppressed [7–11]. Perrett and colleagues were the first to describe neurons in the superior temporal sulcus (STS) that are tuned to different gaze, head and body orientations [9], without any behavioral relevance, however. Other studies have found related results concerning the representation of gaze particularly in the right temporal cortex [13–15], which dominates the processing for visual face perception[16] (cf. Nummenmaa & Calder [17] for a review).

In a series of behavioral, fMRI, and electrophysiological studies our group investigated the psychophysical properties and neural underpinnings of gaze-following behavior in macaques and humans. In this work we identified a circumscribed region in the posterior temporal cortex of humans and macaques, baptized the *gaze following patch* (*GFP*), that is comparatively more active during gaze following than in control conditions characterized by very similar visual and motor demands, yet lacking the need to follow gaze [11,18–25]. This characteristic makes the GFP a candidate for Baron-Cohen's EDD. The distinctive feature of our experimental design was that it required *active* gaze following, i.e. participants did not only passively observe a face gazing in a certain direction but had to utilize it to identify a target among distractors and to subsequently shift their own visual attention to it. In the control condition that we used the target had to be identified based on the iris-color [21] or the identity [25] of the stimulus face. We found that the GFP revealed by contrasting gaze-following and iris-color matching is distinct from the face patch system [21,26,27], albeit close to the middle face patch. Moreover, it is located close to the MT+ complex, a set of areas including the middle temporal area (MT), involved in the processing of visual motion, and may in fact be identical with or a specific part of MT+ as delineated with standard motion stimuli. This is a possibility as the gaze stimuli we used consisted of two images presented in succession, thereby giving the impression of a gaze saccade – i.e., high speed motion of the eyes – requiring attention. Although the control condition involved the same motion component, it was behaviorally irrelevant as it was the iris-color that participants had to exploit. Thus, it may well be that the event that triggers the GFP activity is not the actual retrieval and use of the gaze direction, but that the GFP activity is a correlate of attending to the associated movement of the eyes, i.e. it may reflect the attentive processing of motion independent of whether it is eyes or other objects that move [28]. This possibility is supported by the anatomical proximity of the GFP to the MT+ region (see Figure 2). Here we will test if the GFP must be conflated with the visual motion processing system or whether the GFP fulfills the criterion of domain specificity thereby testing one of the central tenets of Baron-Cohen's Mindreading-

System. The latter is possible because our previous and the current experiment are specifically designed to reveal an EDD by capturing the full-behavioral relevance of gaze-following behavior.

In experiment 1 we will investigate whether the GFP is only activated during gaze following or if a non-social spatial cue that involves motion results in a comparable activation. To this end, we will complement the two conditions that characterize the paradigm that we adopted from Marquardt et al. [21] by a third one involving non-social motion. With this, the experiment consists of *gaze-direction following*, *iris-color mapping* and *cube-orientation following* (see Figure 1); from here on, we will refer to these conditions as *Gaze*, *Iris,* and *Cubes*. *Gaze* requires the participant to track a change in gaze direction, *Iris* a change of iris-color, and *Cubes* a rotation of two cubes. We will investigate the BOLD correlate of neuronal activity evoked in these three experimental conditions using fMRI in healthy human subjects. In experiment 1, participants will view a face displayed on a screen with two cubes superimposed above and below the nasal root respectively. Beneath the face are three differently colored rectangles that serve as gaze targets, one in the center and the other two at ~9 deg eccentricity left and right to it respectively. In each trial, the direction of gaze, the color of the iris, and the orientation of the cubes change to indicate one of the rectangles to which participants are asked to direct their gaze to. Which of the three cues must be used in each trial will be communicated to participants via auditory commands. With this design we will be able to replicate our former findings by computing the defining BOLD contrast of the GFP, *Gaze – Iris,* and infer the associated region of interest (ROI) which is then used to answer *Question 1.1* and *1.2*: Is there a difference between the activity related to *Gaze* and *Cubes* in the left or right GFP? The corresponding null-hypotheses are $H_0^{Q1.1}$: $\Delta\beta_{\text{GFP-left}}^{Gaze-Cube} = 0$ and $H_0^{Q1.2}$: $\Delta\beta_{\text{GFP-right}}^{Gaze-Cubes} = 0$. If the data will demonstrate that contrary to the null-hypotheses *Gaze* related activity is stronger than *Cubes* related activity $\Delta\beta_{\text{GFP-left}}^{Gaze-Cube} > 0$) the existence of the GFP proper would be supported. The reverse effect ($\Delta\beta_{\text{GFP-left}}^{Gaze-Cube} < 0$) or evidence supporting the null-hypothesis of no difference would support that the GFP is not a specialized gaze-module. Since the processing of face perception occurs dominantly in the right hemisphere, we are also

interested in the question whether this is reflected in a hemispheric dominance of *Gaze (*and *Cubes)*. For this, in *Question 2* we will test the null-hypotheses $H_0^{Q2.1}$: $\Delta\beta_{Gaze}^{\mathrm{RH-LH}} = 0$ and $H_0^{Q2.2}$: $\Delta\beta_{Cubes}^{\mathrm{RH-LH}} = 0$.

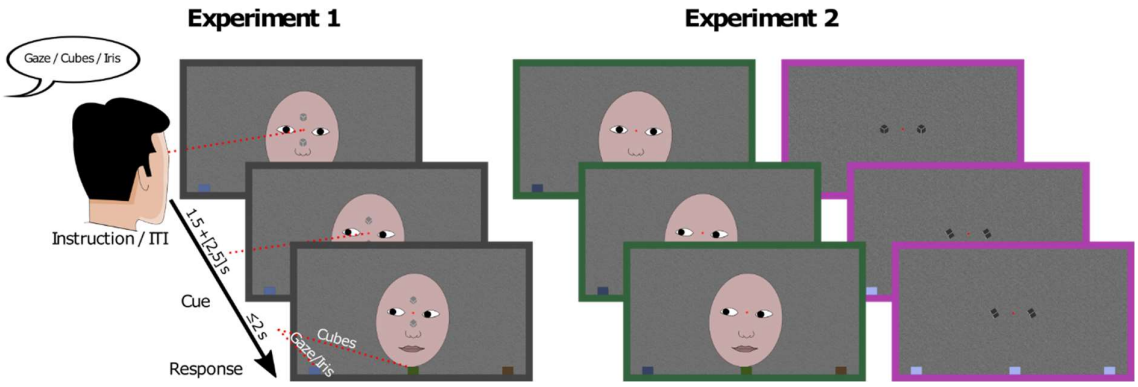

Figure 1 - Illustration of experiment 1 and 2. In the example of experiment 1 the cubes indicate the middle target and the gaze as well as the iris-color the left target. Depending on the instruction, the participant will have to choose the respective target. In experiment 2 the two stimulus components *Gaze* and *Cubes* are presented separately. In the experiment the schematic face shown here is replaced by a photo of a person.

However, even if we will find that the GFP is more strongly activated during *Gaze* as compared to *Cubes* trials, this will not rule out a decisive role of the low-level motion information characterizing the gaze shift. Less GFP activity evoked by cube motion might be a consequence of stimulating different locations in the visual field and thereby different parts of MT+ [29,30]. Although presented at the same eccentricity as the eyes, the two cubes are arranged on the vertical meridian rather than appearing on the horizontal meridian. To investigate the possibility that the GFP is identical to or a part of MT+, participants will participate in a second experiment in which the gazing person (*Gaze-only*) and the cubes devoid of the face in the background (*Cubes-only*) are presented separately but at matching positions of the visual field (see Figure 1). That means that participants either see a face that shifts eye gaze or cubes that rotate presented in the same positions as the eyes. In this way, we can ensure that any activity we detect is due only to the stimulus currently present rather than triggered by the passive perception of the other stimulus with which it appears combined in experiment 1.

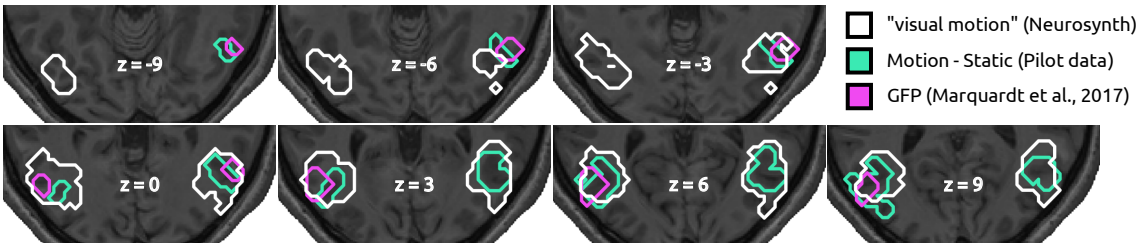

Figure 2 Anatomical locations of motion related areas and the GFP. Shown are transversal cuts from $\mathbf{z = -9}$ to $\mathbf{z = 9}$ in steps of **3 mm**. Locations given by the neurosynth **[31]** database when searching for "visual motion" are outlined in white. The result of the MT localizer of Pilot 1 is outlined in cyan and the GFP from Marquardt et al. **[21]** is outlined in pink.

A well-established response property of the human visual motion processing system are lateralized responses to peripheral motion cues with stimuli in the left hemifield evoking stronger responses in right MT+ and vice versa [32]. Motion in the periphery of the observer´s visual field is elicited by the backward movement of the model´s eyes and the cubes respectively to the central starting position while the observer still fixates the respective target (see Figure 2). On the other hand, the available evidence does not suggest a similar lateralization of gaze following related activity.

On this ground, we will investigate the functional relationship between the GFP and MT+ by analyzing the correlation between hemodynamic response functions (HRFs) of the *Gaze-only* and *Cubes-only* conditions estimated for individual targets. Resorting to correlations rather than to a comparison of beta values immunizes the analysis against potential differences in the baseline activity due to the differences in the visual properties of the stimuli in the two conditions. This approach is backed by studies on non-human primates describing MT/ MST neurons to be primarily tuned to retinal position, direction, speed, and size of the motion stimulus. Size may be relevant due to surround suppression, a mechanism not relevant in our case where the background of the eyes – the face – is static [32]. Thus, we will be able to reveal correspondences/ divergences between the temporal response patterns to the sequence of motion events in the stimuli which are independent of the surroundings of the stimuli. The rationale is that if it is the

special properties of the gaze stimulus that drives the GFP, responses to Gaze-only and Cubes-only will not be correlated. If, however, it rather is the low-level motion pattern that triggers responses, they will be correlated because retinal position, direction, and speed of the motion of the eyes and cubes match. Figure 2 illustrates this concept based on pilot data that yielded patterns reflecting lateralized responses to the low-level motion components. Table 1 shows the condition/target-pairs grouped by predictions of the strength of the correlation if either the conditions are determinant (within-condition compared to cross-condition pairs, grey and red dots) or if laterality/ low-level motion is determinant (blue and yellow circles). As a positive control we will conduct the same analysis based on the individual MT+ ROIs from a localizer paradigm that each participant will perform and test if the correlation patterns provided by the GFP diverge or are congruent with the MT+ patterns. If we will find that for the MT+ ROI the outcome deviates from the latter expectation this result would prohibit further conclusions about whether the GFP is (part of) MT+. In detail, we will estimate 24 HRFs (2 ROIs × 2 hemispheres × 2 conditions × 3 targets) for each participant and analyze them to see whether target ID in conjunction with hemisphere or condition affects the level of correlation in MT+ (*Question 3.1/ 3.2*) and the GFP (*Question 4.1/ 4.2*). Furthermore, we will directly compare the results obtained for MT+ and the GFP by testing whether the correlation coefficients of the HRF pairs have comparable values in both ROIs, i.e., whether they are correlated (*Question 5*). The expected result for MT+ is that those HRF-pairs that account for the lateralization (blue circles in Table 1) characterized by an additional late deflection of the HRF due to the presence of peripheral motion at the end of each trial will be more strongly correlated than those that ignore lateralization (yellow circles ibid.) ($H_1^{Q3.1}$). Furthermore, we expect that MT+ is not modulated by condition and that we will therefore not find any differences between cross-condition correlations (red dots ibid.) and within-condition correlations (gray dots ibid.) ($H_0^{Q3.2}$). On the other hand, the hypothesis that the GFP is a specialized module dedicated to the processing of gaze will be supported if we find evidence that responses to *Gaze-only* and *Cubes-only* are not or significantly less correlated than within-condition pairs ($H_1^{Q4.2}$). If this turns out to be the case and the

expectation for the MT+ ROI is met, it will also be reflected in a lack of correlation between the two ROIs, indicating a functional segregation (H_0^{Q5}). If, however, we will find that the GFP yields the same pattern as the one expected for the MT+ ROI the hypothesis that the GFP is (part of) MT+ would be supported (evidence for $H_1^{Q4.1}$ and for $H_0^{Q4.2}$, as well as for H_1^{Q5}).

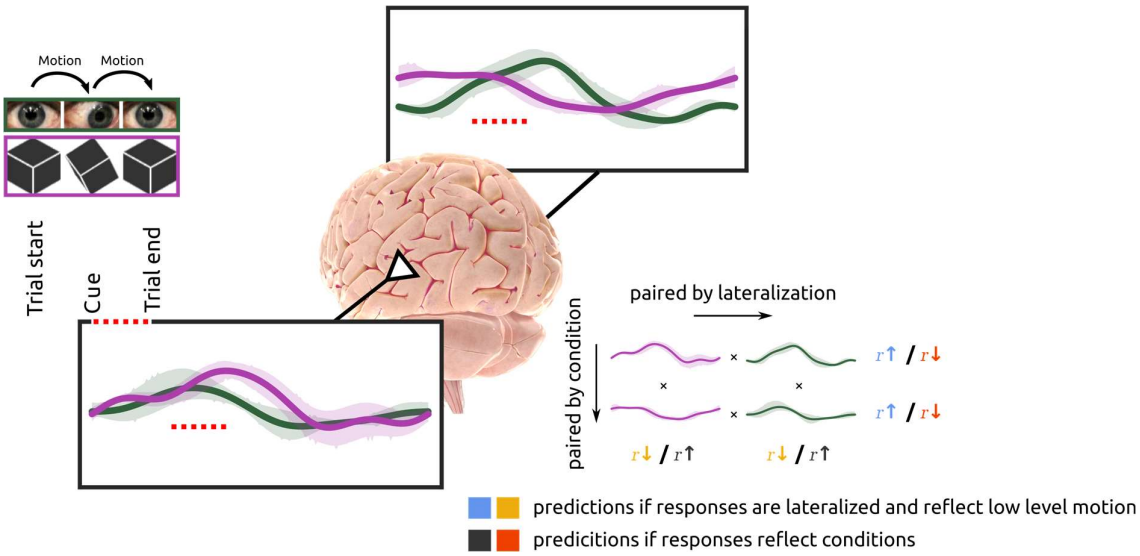

Figure 3 Illustration for Q3 and Q4. Shown are 4 example HRFs from one pilot subject to illustrate the analysis and predictions of experiment 2. In the Gaze-condition the participant looked at the right target such that the second motion event occurred in her left visual hemifield triggering a larger and longer lasting response in the right hemisphere compared to the left hemisphere (green curves). In the Cubes-condition the participant fixated the left target leading to the opposite pattern (purple curves). Computing the correlations between the responses yields results that are in line with the blue and yellow predictions, indicating that the low-level motion components in the stimuli triggers lateralized responses. The shaded areas represent the 95% CI of the HRF estimates. See Table 1 for a full list of the predictions for all relevant response pairs.

Finally, *Question 6* combines Q1, Q3, Q4 (and Q5) to provide the full perspective on the question whether the GFP is (a) a specialized module for gaze processing and (b) distinct from MT+. For (a) and (b) to be true, all of the following conditions will have to be met: *Gaze*-related activity must be greater than *Cubes*-related activity in the GFP (Q1). Target ID in conjunction with

hemisphere must predict high and low correlations in MT+ (Q3.1). Within- and cross-condition correlations must be similar in MT+ (Q3.2). Target ID in conjunction with hemisphere must not predict high and low correlations in the GFP (Q4.1). And finally, the cross-condition correlation must be significantly smaller than the within-condition correlations in the GFP (Q4.2) which implies that the correlation patterns in the GFP and MT+ would not be correlated (Q5). In short Q1: $\Delta\beta_{\mathrm{GFP}}^{Gaze-Cube} > 0 \wedge$ Q3.1: $\Delta\rho_{\mathrm{MT+}}^{\mathrm{low-high}} < 0 \wedge$ Q3.2: $\Delta\rho_{\mathrm{MT+}}^{\mathrm{within-acros}} = 0 \wedge$ Q4.1: $\Delta\rho_{\mathrm{GFP}}^{\mathrm{low-high}} = 0 \wedge$ Q4.2: $\Delta\rho_{\mathrm{GFP}}^{\mathrm{within-acros}} > 0 \wedge$ Q5: $\rho_{\mathrm{MT+/GFP}} = 0$. At this point, we want to emphasize the importance of Q1 to answer Q6 even though the correlation analysis in Q4 and Q5 may appear to be sufficient. However, a possible experimental result exists that would lead to incorrect conclusions if based on correlations alone. Namely, if the GFP ROI does not provide any task-related signal in the *Gaze-only* (or *Cubes-only*) condition at all. Then, the within-condition correlations will necessarily be higher than the cross-condition correlations due to spurious correlations. In addition, lateralization would not matter, as well. If Q6 would be answered negatively, *Question 7* combines Q1, Q3, Q4 and Q5 to assess if the relevant stimulus component triggering the activity in the GFP is motion, i.e., if the GFP is (part of) MT+. This can be concluded if (Q1) the *Cubes*-related activity is equal to or larger than the *Gaze*-related activity, (Q3.1/4.1) both, MT+ and the GFP, show the same correlation patterns that are predicted by lateralized responses to the peripheral motion cues as well as (Q3.2/4.2) that both ROIs do not show any differences between across-condition and within-condition correlations implying that the correlation patterns in both ROIs are correlated (Q5). In short Q1: $\Delta\beta_{\mathrm{GFP}}^{Gaze-Cube} \leq 0 \wedge$ Q3.1/ 4.1: $\Delta\rho_{\mathrm{MT}}^{\mathrm{low-high}} < 0 > \Delta\rho_{\mathrm{GFP}}^{\mathrm{low-high}} \wedge$ Q3.2/ 4.2: $\Delta\rho_{\mathrm{MT+}}^{\mathrm{within-acro}} = 0 = \Delta\rho_{\mathrm{GFP}}^{\mathrm{within-acro}} \wedge$ Q5: $\rho_{\mathrm{MT+/GFP}} > 0$. Lastly, we want to point out once more that if the results regarding *Question* 3 will be not in line with the expectations from a visual motion area, conclusions regarding the nature of the GFP can only be based on the comparison between *Gaze* and *Cubes* related activity within the GFP in experiment 1. This means equally high or higher activity in the *Cubes* condition as compared to the *Gaze* condition would still provide evidence against the GFP proper. However, larger *Gaze* related activity alone is not sufficient to rule out the possibility that the GFP is a

subpart of MT+ and that differences between *Gaze* and *Cubes* related activity may reflect the retinotopic differences in the stimuli.

Table 1 Correlations coefficients will be computed for all marked pairs. For pairs marked by blue circles correlation coefficients are expected to be higher than for those marked by yellow circles if responses are lateralized and triggered by low-level motion components (Q3.1/ 4.1). If, however, responses reflect the conditions (Q3.2/ 4.2), then correlation coefficients for pairs marked by dark grey dots will be greater than those marked by red dots. Target-2 trials (middle) are only paired with itself to consistently maintain lateralization with respect to the left and right targets. The analysis will be carried out on data of the GFP and MT+ (ROI = [GFP, MT]). Left and right refers to the hemisphere. *GO* = *Gaze-only*, *CO* = *Cubes-only*; the number refers to the target ID: 1 – left target, 2 – middle target and 3 – right target.

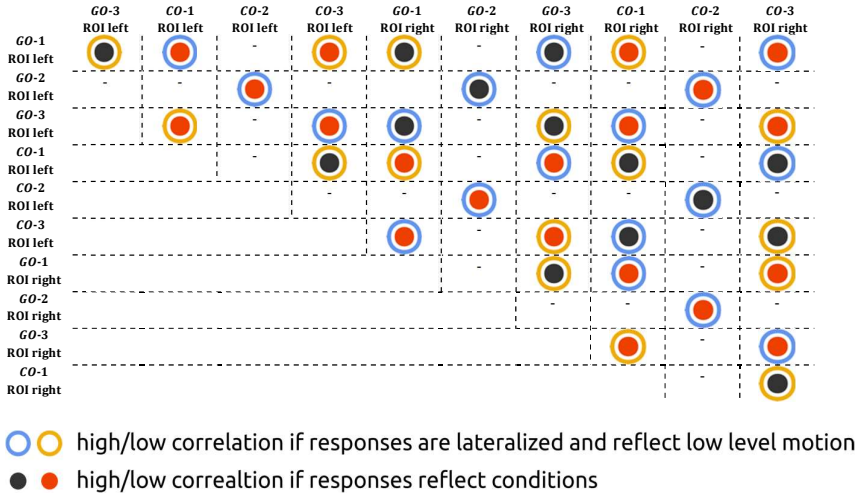

Summary table

Question	Null Hypothesis	Outcome Measures	Sampling plan	Analysis Plan	Interpretation of outcomes
Q1 Is the GFP-ROI differentially activated during *Gaze* and *Cubes* in experiment 1?	$H_0^{Q1.1}: \Delta\beta_{\text{GFP-left}}^{Gaze-Cubes} = 0$ $H_0^{Q1.2}: \Delta\beta_{\text{GFP-right}}^{Gaze-Cubes} = 0$	Beta estimates of BOLD signal	$BF_{01/10}^{Q1} \geq 10$	Bayesian hierarchical model	**1.** $\Delta\boldsymbol{\beta}_{\mathbf{GFP}}^{\boldsymbol{Gaze-Cubes}} \leq \mathbf{0}$: no difference between *Gaze* and *Cubes* related activity or less *Gaze* related activity in the GFP. Support against the hypothesis that the GFP is a specialized module for gaze-following. **2** $\Delta\boldsymbol{\beta}_{\mathbf{GFP}}^{\boldsymbol{Gaze-Cubes}} > \mathbf{0}$: The GFP is stronger activated during *Gaze* trials than during *Cubes* trials. Either the GFP is a specialized gaze-following module or it is a subpart of MT+ reflecting retinotopic locations. These possibilities are disentangled in Q6.
Q2 Is there a hemispheric dominance for *Gaze* or *Cubes*?	$H_0^{Q2.1}: \Delta\beta_{Gaze}^{\text{RH-LH}} = 0$ $H_0^{Q2.2}: \Delta\beta_{Cubes}^{\text{RH-LH}} = 0$	Beta estimates of BOLD signal	$BF_{01/10}^{Q2} \geq 10$	Bayesian hierarchical model	**1.** $\Delta\boldsymbol{\beta}_{\boldsymbol{Gaze/Cubes}}^{\mathbf{RH-LH}} = \mathbf{0}$: no difference between between the left and right hemisphere. **2.** $\Delta\boldsymbol{\beta}_{\boldsymbol{Gaze/Cubes}}^{\mathbf{RH-LH}} > \mathbf{0}$: The right hemisphere is stronger activated than the left hemisphere. Complies with the right hemispheric dominance of visual face processing. **3.** $\Delta\boldsymbol{\beta}_{\boldsymbol{Gaze/Cubes}}^{\mathbf{RH-LH}} < \mathbf{0}$: The left hemisphere is stronger activated than the right hemisphere.
Q3.1 Does target ID in conjunction with hemisphere affect	$H_0^{Q3.1}: \Delta\rho_{\text{MT+}}^{\text{low-high}} = 0$	Correlation coefficients of HRF estimates of BOLD signals	$BF_{01/10}^{Q3.1} \geq 10$	Bayesian hierarchical model	**1.** $\Delta\boldsymbol{\rho}_{\mathbf{MT+}}^{\mathbf{low-high}} = \mathbf{0}$: no lateralized response in MT+. Either misspecified ROI or the peripheral motion cue is not of relevance. Invalidates analysis of experiment 2.

the level of correlations in MT+.					**2.** $\Delta\boldsymbol{\rho}_{\mathbf{MT+}}^{\mathbf{low-high}} < \mathbf{0}$: result matches the prediction based on lateralization. **3.** $\Delta\boldsymbol{\rho}_{\mathbf{MT+}}^{\mathbf{low-high}} > \mathbf{0}$: reverse effect as predicted (implausible). Invalidates analysis of experiment 2.
Q3.2 Does condition affect the level of correlation in MT+. Q3.1 and 3.2 are positive controls for the second part of the analysis. Any result not matching the prediction invalidates the analysis of experiment 2.	$H_0^{Q2.2}: \Delta\rho_{\mathrm{MT+}}^{\mathrm{within-across}} = 0$	Correlation coefficients between HRF estimates of BOLD signals	$BF_{01/10}^{Q3.2} \geq 10$	Bayesian hierarchical model	**1.** $\Delta\boldsymbol{\rho}_{\mathbf{MT+}}^{\mathbf{within-across}} = \mathbf{0}$: correlations within conditions and across conditions are equally strong. Matches the prediction for a visual motion area. **2.** $\Delta\boldsymbol{\rho}_{\mathbf{MT+}}^{\mathbf{within-across}} < \mathbf{0}$: correlations within conditions smaller than across conditions (implausible). Invalidates analysis of experiment 2. **3.** $\Delta\boldsymbol{\rho}_{\mathbf{MT+}}^{\mathbf{within-across}} > \mathbf{0}$: correlations within conditions larger than across conditions. Activity patterns are not purely reflecting the sequence of motion events in the stimuli. Invalidates analysis of experiment 2.
Q4.1 Does target ID in conjunction with hemisphere affect the level of correlations in the GFP	$H_0^{Q4.1}: \Delta\rho_{\mathrm{GFP}}^{\mathrm{low-high}} = 0$	Correlation coefficients between HRF estimates of BOLD signals	$BF_{01/10}^{Q4.1} \geq 10$	Bayesian hierarchical model	**1.** $\Delta\boldsymbol{\rho}_{\mathbf{GFP}}^{\mathbf{low-high}} = \mathbf{0}$: no lateralized response in GFP. Given that $\Delta\boldsymbol{\rho}_{\mathbf{MT+}}^{\mathbf{low}} < \mathbf{0}$, we will conclude that the GFP is functionally different from MT+. See Q6 for full interpretation. **2.** $\Delta\boldsymbol{\rho}_{\mathbf{GFP}}^{\mathbf{low-high}} < \mathbf{0}$: result matches the prediction based on lateralization. Given that $\Delta\boldsymbol{\rho}_{\mathbf{MT+}}^{\mathbf{low}} < \mathbf{0}$, we will conclude that the GFP and MT+ are functionally homologous. See Q6 for full interpretation. **3.** $\Delta\boldsymbol{\rho}_{\mathbf{GFP}}^{\mathbf{low-high}} > \mathbf{0}$: reverse effect as prediction (implausible). See Q6 for full interpretation.

Q4.2 Does condition affect the level of correlation in the GFP	$H_0^{Q4.2}: \Delta\rho_{\text{GFP}}^{\text{same}} = 0$	Correlation coefficients of HRF estimates of BOLD signals	$BF_{01/10}^{Q4.2} \geq 10$	Bayesian hierarchical model	**1.** $\boldsymbol{\Delta\rho_{\text{GFP}}^{\text{same}} = 0}$: both conditions elicit the same responses in GFP. Indicating that it is not a specialized module for the processing of gaze. See Q6 for full interpretation. **2.** $\boldsymbol{\Delta\rho_{\text{GFP}}^{\text{same}} < 0}$: lower correlation within- than across-conditions (implausible). **3.** $\boldsymbol{\Delta\rho_{\text{GFP}}^{\text{same}} > 0}$: across-conditions pairs are less correlated than within-condition pairs. Supporting that the GFP is a specialized module. See Q6 for full interpretation.
Q5 are the correlation coefficients from the GFP correlated with those from MT+	$H_0^{Q4}: \rho_{\text{MT+/GFP}} = 0$	Correlation coefficients	$BF_{01/10}^{Q5} \geq 10$	Bayesian correlation test	**1.** $\boldsymbol{\rho_{\text{MT+/GFP}} = 0}$: no correlation between MT+ and GFP. GFP is functionally segregated from MT+. **2.** $\boldsymbol{\rho_{\text{MT+/GFP}} > 0}$: GFP is (part of) MT+ **3.** $\boldsymbol{\rho_{\text{MT+/GFP}} < 0}$: GFP and MT+ are anticorrelated (implausible).
Q6 Is the GFP (a) a specialized module for the processing of gaze and (b) functionally segregated from MT+?	-	-	-	Combination of Q1,3,4,5	In order to conclude that the GFP is a specialized module the following results must occur: (a) Q1: $\Delta\beta_{\text{GFP}}^{Gaze-Cubes} > 0$ (b) Q3.1: $\Delta\rho_{\text{MT}}^{\text{low-high}} < 0$ Q3.2: $\Delta\rho_{\text{MT+}}^{\text{within-across}} = 0$ Q4.1: $\Delta\rho_{\text{GFP}}^{\text{low-high}} = 0$ Q4.2: $\Delta\rho_{\text{GFP}}^{\text{within-across}} > 0$ Q5: $\rho_{\text{MT+/GFP}} = 0$

Q7 Is the GFP identical with or a part of MT+?	-	-	-	Combination of Q1,3,4,5,6	In order to conclude that the relevant stimulus component triggering activity in the GFP is motion and that it cannot be distinguished from MT+ the following results must occur: Q1: $\Delta\beta_{\mathrm{GFP}}^{Gaze-Cubes} \leq 0$ Q3.1/ 4.1: $\Delta\rho_{\mathrm{MT}}^{\mathrm{low-high}} < 0 > \Delta\rho_{\mathrm{GFP}}^{\mathrm{low-high}}$ Q3.2/ 4.2: $\Delta\rho_{\mathrm{MT+}}^{\mathrm{within-across}} = 0 = \Delta\rho_{\mathrm{GFP}}^{\mathrm{within-across}}$ Q5: $\rho_{\mathrm{MT+/GFP}} > 0$

Methods

Ethical Approval Plan

The research plan presented here is approved by the Ethics Board of the Medical Faculty, University of Tübingen, Germany and will be conducted in accordance with the principles of human research ethics of the Declaration of Helsinki. Written consent will be obtained from all participants, and they will be compensated with a lump sum of 40€.

Design

Setup and general procedure

The study consists of two experimental and two localizer tasks distributed over two separate fMRI sessions on different days. We will acquire MR images using a 3T scanner (Siemens Magnetom Prisma) with a 20-channel phased array head coil. The head of the subjects will be fixed inside the head coil by using plastic foam cushions to avoid head movements. An AutoAlign sequence will be used to standardize the alignment of images across sessions and subjects. A high-resolution T1-weighted anatomic scan (MP-RAGE, 176 × 256 × 256 voxel, voxel size 1 × 1×1 mm) and local field maps will be acquired. Functional scans will be conducted using a $T2^*$-weighted echo-planar multibanded 2D sequence (multiband factor = 2, TE = 35 ms, TR = 1500 ms, flip angle = 70°) which covers the whole brain (44 × 64 × 64 voxel, voxel size 3 × 3 × 3 mm, interleaved slice acquisition, no gap).

Participants will lie in the scanner and view the stimulus monitor that is placed at its head-end via a mirror system. The distance between the participant and the monitor is ~190 cm and it covers ~20° of the field of view in the horizontal and ~12° in the vertical. In the session with experiment 1 participants will wear air pressure headphones. The stimuli and data collection will be controlled via a custom software package [33].

Experiment 1

In each trial of experiment 1 (see Figure 1) participants will see a photograph of the face of a female with superimposed cubes and a red fixation dot positioned on the nasion. The size of the cubes will match the size of the irises, and they will be arranged so that they are equidistant from the nasion in the vertical direction as the eyes are in the horizontal direction. Each trial will start with a verbal instruction delivered via headphones during which the face is looking towards the participant, her iris color is greyish, and the cubes point straight ahead with one of their vertices. The verbal instruction will either be *Gaze*, *Cubes,* or *Iris* indicating which of the upcoming cues must be used to identify the target rectangle among three differently colored rectangles at the bottom of the stimulus image. After a variable ITI between 2 and 5 s during which participants will have to fixate the central fixation dot the face makes a gaze shift towards one of the rectangles, her iris color changes to match one of the target colors and the cubes rotate such that the frontal vertex points towards one of the targets. Upon these cues, participants are asked to react as quickly as possible with a saccade to the respective target, and to hold the fixation there until the next trial starts. The beginning of the next trial is indicated by the return of the cues to their initial state and the next instruction. Each trial lasts between 5.5 and 8.5 s, and participants perform 7 runs à 81 trials, within which targets, and instructions are randomized i.e., we employ an event-related design. Between runs participants can rest.

Experiment 2

In experiment 2 the face and the cubes will be presented separately (*Gaze-only*, *Cubes-only*), and *Iris* will be omitted here as a cue entirely (see Figure 1). Also, at the beginning of each trial there will be no instruction since participants only see either the face or the cubes. In each run only one type of cue (*Gaze* or *Cubes*) will be presented, the targets will be randomized, and participants will perform 4 runs à 81 trials of each. Otherwise, the task and the temporal sequence will be the same as in experiment 1.

Motion localizer

To localize the complex of motion processing areas (MT+) participants will participate in a standard motion localizer task in which they alternately view (random) dot motion and a static dot pattern while keeping fixation on a central fixation dot. Both, the moving and the static dots will be presented 15 times per run for 15 seconds each. In total, participants will conduct 6 runs during the first and second session. The dot field will have a size of 7 deg, consist of 200 dots with a dot size of 0.1 deg and a lifetime of 500 ms. The lifetimes of individual dots will be unsynchronized. In case of the "moving dots" stimulus individual dots will move at a speed of 1.5 deg/s. In 3 out of the 6 runs the dots will move individually in random directions (noise level of 100%) and in the other 3, coherently (noise level of 0%) in a direction randomly drawn without replacement from a vector specifying 45 possible directions evenly sampling 360 deg.

Sampling plan

We will employ Bayesian methods for analysis. In line with the requirements for registered reports we will include further participants until all computed Bayes Factor reach the threshold for *strong evidence* of 10 in favor of the null- or the alternative hypothesis. Pilot data suggests that a small number of participants will be sufficient, as most of the BFs we calculated have already reached this level with just two pilot participants. Note that throughout this manuscript Bayes Factors are reported as $\log_{10}$ transforms, although this is not specified everywhere to improve readability. Furthermore, Bayes Factors will always be reported from the perspective of the null hypothesis (BF_{01}), this implies that values above 1 correspond to *strong evidence* in favor of the null hypothesis and values below -1 on favor of the alternative hypothesis. The exclusion of data will be based solely on the observed behavior of the subject during the experiment. We will observe the participants performing the tasks with a camera and record their answers, i.e., the direction of their response saccades, in writing for each trial. This is necessary since eye-tracking quality within the fMRI scanner is often not stable enough. Before data analysis we will examine participants' responses and exclude runs that contain more than 10% of false responses and exclude a participant completely if this applies to more than two runs of any condition.

Analysis Plan

Preprocessing

We will use the software package *fMRIPrep* (ver. 20.2.1) [34,35] (RRID:SCR_016216) which is based on *Nipype* 1.5.1 [36] (RRID:SCR_002502) to preprocess the fMRI data. The following sections describing the preprocessing are boilerplates automatically generated by *fMRIPrep* for the pilot data and inserted unchanged. For the main data set we will employ the exact same pipeline.

Anatomical data preprocessing

A total of 1 T1-weighted (T1w) images were found within the input BIDS dataset. The T1w image was corrected for intensity non-uniformity (INU) with N4BiasFieldCorrection , distributed with ANTs 2.3.3 [38] (RRID:SCR_004757), and used as T1w-reference throughout the workflow. The T1w-reference was then skull-stripped with a *Nipype* implementation of the antsBrainExtraction.sh workflow (from ANTs), using OASIS30ANTs as target template. Brain tissue segmentation of cerebrospinal fluid (CSF), white-matter (WM) and gray-matter (GM) was performed on the brain-extracted T1w using fast [39] (FSL 5.0.9, RRID:SCR_002823). Brain surfaces were reconstructed using recon-all [40] (FreeSurfer 6.0.1, RRID:SCR_001847), and the brain mask estimated previously was refined with a custom variation of the method to reconcile ANTs-derived and FreeSurfer-derived segmentations of the cortical gray-matter of Mindboggle [41] (RRID:SCR_002438). Volume-based spatial normalization to one standard space (MNI152NLin2009cAsym) was performed through nonlinear registration with antsRegistration (ANTs 2.3.3), using brain-extracted versions of both T1w reference and the T1w template. The following template was selected for spatial normalization: *ICBM 152 Nonlinear Asymmetrical template version 2009c* [42] (RRID:SCR_008796; TemplateFlow ID: MNI152NLin2009cAsym).

Functional data preprocessing

For each of the runs found per subject (across all tasks and sessions), the following preprocessing will be performed. First, a reference volume and its skull-stripped version were

generated by aligning and averaging 1 single-band references (SBRefs). A B0-nonuniformity map (or *fieldmap*) was estimated based on a phase-difference map calculated with a dual-echo GRE (gradient-recall echo) sequence, processed with a custom workflow of *SDCFlows* inspired by the epidewarp.fsl script [43] and further improvements in HCP Pipelines [44]. The *fieldmap* was then co-registered to the target EPI (echo-planar imaging) reference run and converted to a displacements field map (amenable to registration tools such as ANTs) with FSL's fugue and other *SDCflows* tools. Based on the estimated susceptibility distortion, a corrected EPI (echo-planar imaging) reference was calculated for a more accurate co-registration with the anatomical reference. The BOLD reference was then co-registered to the T1w reference using bbregister (FreeSurfer) which implements boundary-based registration [45]. Co-registration was configured with six degrees of freedom. Head-motion parameters with respect to the BOLD reference (transformation matrices, and six corresponding rotation and translation parameters) are estimated before any spatiotemporal filtering using mcflirt [46] (FSL 5.0.9). BOLD runs were slice-time corrected using 3dTshift from AFNI 20160207 [47] (RRID:SCR_005927). First, a reference volume and its skull-stripped version were generated using a custom methodology of *fMRIPrep*. The BOLD time-series (including slice-timing correction when applied) were resampled onto their original, native space by applying a single, composite transform to correct for head-motion and susceptibility distortions. These resampled BOLD time-series will be referred to as *preprocessed BOLD in original space*, or just *preprocessed BOLD*. The BOLD time-series were resampled into standard space, generating a *preprocessed BOLD run in MNI152NLin2009cAsym space*. Several confounding time-series were calculated based on the *preprocessed BOLD*: framewise displacement (FD), DVARS and three region-wise global signals. FD was computed using two formulations following Power (absolute sum of relative motions [48]) and Jenkinson (relative root mean square displacement between affines [46]). FD and DVARS are calculated for each functional run, both using their implementations in *Nipype* (following the definitions by Power [48]). The three global signals are extracted within the CSF, the WM, and the whole-brain masks. Additionally, a set of physiological regressors were extracted

to allow for component-based noise correction (*CompCor* [49]). Principal components are estimated after high-pass filtering the *preprocessed BOLD* time-series (using a discrete cosine filter with 128s cut-off) for the two *CompCor* variants: temporal (tCompCor) and anatomical (aCompCor). tCompCor components are then calculated from the top 2% variable voxels within the brain mask. For aCompCor, three probabilistic masks (CSF, WM and combined CSF+WM) are generated in anatomical space. The implementation differs from that of Behzadi et al. [49] in that instead of eroding the masks by 2 pixels on BOLD space, the aCompCor masks are subtracted a mask of pixels that likely contain a volume fraction of GM. This mask is obtained by dilating a GM mask extracted from the FreeSurfer's *aseg* segmentation, and it ensures components are not extracted from voxels containing a minimal fraction of GM. Finally, these masks are resampled into BOLD space and binarized by thresholding at 0.99 (as in the original implementation). Components are also calculated separately within the WM and CSF masks. For each CompCor decomposition, the k components with the largest singular values are retained, such that the retained components' time series are sufficient to explain 50 percent of variance across the nuisance mask (CSF, WM, combined, or temporal). The remaining components are dropped from consideration. The head-motion estimates calculated in the correction step were also placed within the corresponding confounds file. The confound time series derived from head motion estimates and global signals were expanded with the inclusion of temporal derivatives and quadratic terms for each [50]. Frames that exceeded a threshold of 0.5 mm FD or 1.5 standardised DVARS were annotated as motion outliers. All resamplings can be performed with *a single interpolation step* by composing all the pertinent transformations (i.e., head-motion transform matrices, susceptibility distortion correction when available, and co-registrations to anatomical and output spaces). Gridded (volumetric) resamplings were performed using antsApplyTransforms (ANTs), configured with Lanczos interpolation to minimize the smoothing effects of other kernels [51]. Non-gridded (surface) resamplings were performed using mri_vol2surf (FreeSurfer).

Copyright Waiver

The above boilerplate text was automatically generated by *fMRIPrep* with the express intention that users should copy and paste this text into their manuscripts *unchanged*. It is released under the CC0 license.

Run- and first-level GLMs, ROI definition

For each participant we will compute GLMs (general linear models) for each run individually (run-level) as well as a GLM for the combination of all runs (first-level) to obtain the respective β-images for each condition using the Python package *nilearn* [52]. To mitigate the effects of motion artefacts and other noise sources, the nuisance regressors *global_signal*, *csf*, white_matter, *trans_x*, *trans_y*, *trans_z*, *rot_x*, *rot_y*, *rot_z* and their respective first derivatives estimated by *fMRIPrep* will be included in the design matrices. As model for the *HRF* we will use the *glover + derivative + dispersion* provided by *nilearn* and include a polynomial drift model of order 3 to remove slow drifts in the data. Further, we will mask the data with each run's mask image (or the average for the first-level GLM) provided by *fMRIPrep* and apply smoothing with *fwhm* = 5 mm.

To define the GFP and the MT+ ROI the resulting first-level β-images will be used to compute the contrasts $Gaze - Iris$ (experiment 1) and $Motion - Static$ for the localizer task, respectively. For each participant these ROIs will be determined individually by applying the most liberal statistical threshold that allows to differentiate a separable activity patch at the location of the reference coordinates. These are for the GFP $(\mathrm{x} = -55,\ \mathrm{y} = -68,\ \mathrm{z} = 1)$ and $(\mathrm{x} = 50,\ \mathrm{y} = -64,\ \mathrm{z} = -3)$ [18] and for MT+ $(\mathrm{x} = -45,\ \mathrm{y} = 70,\ \mathrm{z} = 3)$ and $(\mathrm{x} = 46,\ \mathrm{y} = -67,\ \mathrm{z} = 4)$. The latter coordinates are the center of the output of a *neurosynth* [31] database search for *visual motion*. All coordinates reported in this study refer to the MNI space. We expect that the GFP ROI will not be identifiable for all participants in the way described above. For these we will construct a spherical ROI with a radius of 8 mm located at the individual local maximum closest to the reference coordinates.

Question 1/ 2: Comparison of Gaze and Cubes related activity in the left and right GFP

We will extract each participant's run-level *Gaze* and *Cubes* β-values from the GFP and average across voxels. Thus, we will obtain 6 values per hemisphere and participant for each condition. These will be fed into a Bayesian hierarchical regression model with *run* and *participant* as nested group-level intercepts and slopes and condition (*Question 1*) or hemisphere (*Question 2*) as the population-level effect. *Participant* will only be added as a group-level effect if the number of participants is > 5 to avoid model fitting problems as it is recommended by different sources (e.g. Bolker et al. [53]). Modeling will be carried out in *R* [54] using the *brms* [55] package. Priors for the generative model were tuned to yield reasonable prior and posterior predictions for the pilot data. As marginal prior for the effect of condition/ hemisphere on the β-values we will use normal distribution with $\mu = 0$, $\sigma = 1$. The *R* code of the model and the priors are reported in the Supplementary Materials section. The model will provide the effect estimate as $\Delta\beta^{Gaze-Cubes}_{\text{GFP-left}}$ which will be positive if the *Gaze* related activity is larger than the *Cubes* related activity, and smaller vice versa. Bayes Factors will be computed via the Savage-Dickey density ratio evaluating the ration between the posterior and the prior at the parameter value of zero [56] and $\log_{10}$ transformed. The terminology used in this study to describe the amount of evidence is adopted from Wetzels et al [57].

Question 3-5: HRF estimation and correlation analysis

For each participant and ROI, we will estimate the *HRF* for each condition and target of experiment 2. This yields 24 HRFs estimates in total for each participant (2 ROIs × 2 hemispheres × 2 conditions × 3 targets). To do so, the mean BOLD signals from the ROIs will be extracted and linear deconvolution will be applied to disentangle the responses to the different conditions/ targets. Prior to signal extractions, the BOLD images will be denoised using the same confounds as for the GLMs (see above), smoothed with *fwhm* = 5 mm, and standardized. For the deconvolution, we will resort to the *nideconv* [58] package using 9 *fourier* regressors as the basis

set which allows a larger flexibility than the canonical HRF while being less complex than a FIR model.

For each ROI, we will compute linear correlation coefficient (employing the function *correlationBF* [59]) between all relevant pairs (see Table 1) of the responses to the left, middle and right target within and across the conditions of experiment 2. In total, we will obtain the correlation coefficients of 34 HRF-pairs for each participant and ROI. These will be grouped by the expected correlation if the responses to the second motion cue in the end of trials are lateralized (color code of the circles in Table 1) and by within- and cross-condition pairings (color code of the dots in Table 1). These groups will be analyzed for differences using Bayesian hierarchical models with a group level effect for *participants* if the number of participants is larger than 5. The correlation coefficients will be modeled as gaussian distributions within the limit of possible values of correlation coefficients – between -1 and 1. Priors for the generative model were tuned to yield reasonable prior and posterior predictions for the pilot data (see Supplementary Material for details). As marginal priors for the effect of the respective groupings we will use a normal distribution with $\mu = 0$ and $\sigma = 2$. The first model will provide the effect estimate as $\Delta\rho_{\mathrm{GFP}}^{\mathrm{low-high}}$ which will be negative if the prediction based on lateralization is met. The second model will provide the effect estimate as $\Delta\rho_{\mathrm{GFP}}^{\mathrm{within-cross}}$ which will be positive if the prediction based on condition is met. Bayes Factors will be computed via the Savage-Dickey method and $\log_{10}$ transformed for report here.

Finally, if the correlation of a pair of HRFs is high in one ROI, we will test whether it is then also high in the other ROI (Q5). We will do so by computing the correlation between the ROIs and the Bayes Factor testing against no correlation using the *correlationBF* function.

Timeline

Data collection will be commenced immediately upon acceptance and is expected to be completed within 2 months. We estimate 1 month for completion of the Stage 2 manuscript.

Pilot data

We collected pilot data from two participants to evaluate our paradigm and analysis plan. The pilot data is not used to develop the hypotheses. Figure 5 shows the individual distributions of the mean β-values of the GFP separated by condition and hemisphere. Testing the effect of condition grouped by hemisphere yields *anecdotal evidence* that *Cubes*-related activity is greater than *Gaze*-related activity in the left hemisphere and *strong evidence* in favor of the null hypothesis of no difference between *Gaze* and *Cubes* in the right hemisphere (LH: $\Delta\beta_{\text{GFP-left}}^{Gaze-Cubes} = -0.92$, $\text{CI}^{95\%}$ = [-1.58, -0.21], $BF_{01}^{Q1.1} = 0.47$; RH: $\beta_{\text{GFP-right}}^{Gaze-Cube} = -0.01$, $\text{CI}^{95\%}$ = [-0.32, -0.35], $BF_{01}^{Q1.2} = 21.96$).

Testing for an effect of hemisphere grouped by condition yields for *Cubes* moderate and for *Gaze extreme evidence* against no difference indicating that in both conditions the right hemisphere is stronger activated than the left hemisphere with a larger effect size in the Gaze condition (*CF*: $\Delta\beta_{Cubes}^{\text{RH-LH}} = 1.73, \text{CI}^{95\%}$ = [0.61, 2.78], $BF_{01}^{Q2} = -0.9$; *GF*: $\beta_{Gaze}^{\text{RH-L}} = 2.65, \text{CI}^{95\%}$ = [1.57, 3.78], $BF_{01}^{Q2} = -3.4$).

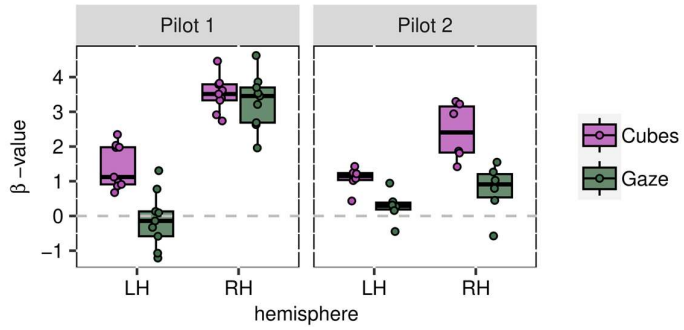

Figure 4 Question 1: distributions of $\boldsymbol{\beta}$-values of the GFP across runs of experiment 1 individually for both pilot subjects. *Gaze*-related values are shown in green and *Cubes*-related in purple. LH and RH mean left and right hemisphere, respectively. Shown are boxplots displaying the median and the interquartile range. Overlayed are violin plots to visualize the densities.

Figure 5 (A) shows the results of the correlation analysis of experiment 2 (Q3/4/5). Data points in the scatter plot correspond to the pairs specified in the Table 1 for the GFP (ordinate) and MT+ (abscissa) ROI. The inlet in the top left corner shows the correlation coefficient and the corresponding *BF* which indicates *strong evidence* in favor of a correlation between the two ROIs for the pilot data. This means that if a pair of responses is correlated in one ROI it tends to be correlated in the other ROI as well. The box-plots show the correlation coefficients grouped by predictions based on the effect of lateralized responses/ low-level motion (blue and yellow) and condition (red and grey). The vertical box plot represents the projection of the data onto the ordinate, i.e., the GFP ROI, and the horizontally oriented one the projection onto the abscissa which represents MT+. The insets show the respective *BF*s of testing for differences. The pilot data suggest for the GFP *moderate evidence* in favor of the presence of an effect of lateralization (Q4.1), *moderate evidence* in favor of the absence of an effect of condition (Q4.2), and for MT+ *extreme evidence* in favor of the presence an effect of lateralization for MT+ (Q3.1) and *moderate evidence* in favor of the absence of an effect of condition (Q3.2).

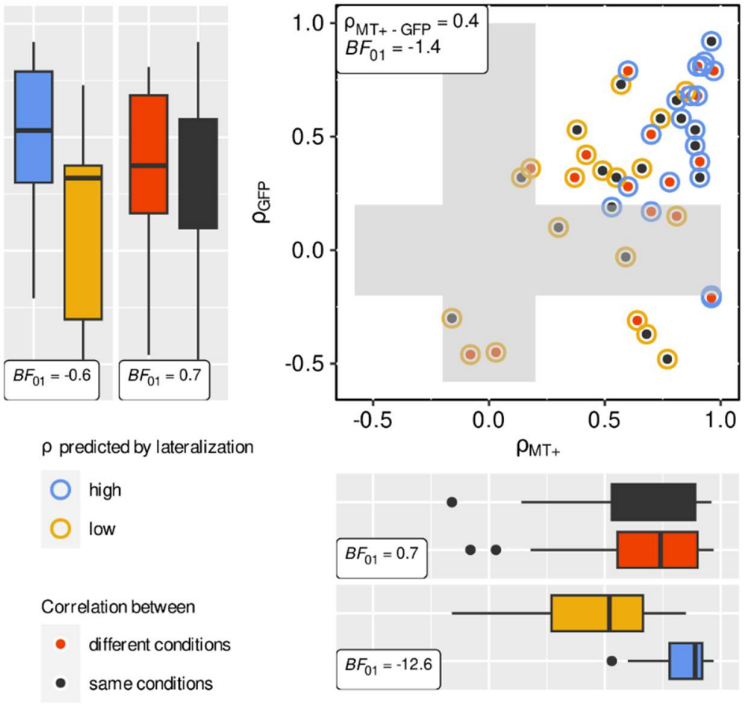

Figure 5 Scatter Plot: Data points correspond to the pairs specified in Table 1 for the GFP (ordinate) and MT+ (abscissa) ROI. There is *strong evidence* for the presence of a correlation between the two ROIs (inlet). The grey shaded area marks the range where there is no *strong evidence* for the presence of a correlation. The box plots represent the projections of the datapoints onto the ordinate (GFP) and abscissa (MT+) grouped by predictions based on lateralization/ low-level motion (blue/ yellow) and condition (red/ grey). Both ROIs show *moderate/ strong evidence* in favor of an effect of lateralization and *moderate evidence* in favor of the absence of an effect of condition. Note, *BF*s are reported as their $\log_{10}$ transform.

Data Availability Plan

Unprocessed data organized in accordance with the BIDS format will be publicly available through OpenNeuro.

Any code used for analysis will be publicly available through GitHub.

References

1. Baron-Cohen S. How to build a baby that can read minds: Cognitive mechanisms in mind reading. Curr Psychol Cogn. 1994;13: 513–552.

2. Baron-Cohen S. The Empathizing System: a revision of the 1994 model of the Mindreading System.

3. Fodor JA. The Modularity of Mind: An Essay on Faculty Psychology. MIT Press; 1983.

4. Panksepp J, Panksepp J. The seven sins of evolutionary psychology. 2001. Available: https://www.semanticscholar.org/paper/The-seven-sins-of-evolutionary-psychology-Panksepp-Panksepp/0dc723dd3998691d164e1eb2057b98411496db38

5. Westlin C, Theriault JE, Katsumi Y, Nieto-Castanon A, Kucyi A, Ruf SF, et al. Improving the study of brain-behavior relationships by revisiting basic assumptions. Trends in Cognitive Sciences. 2023;27: 246–257. doi:10.1016/j.tics.2022.12.015

6. Emery NJ. The eyes have it: The neuroethology, function and evolution of social gaze. Neuroscience & Biobehavioral Reviews. 2000;24: 581–604. doi:10.1016/S0149-7634(00)00025-7

7. Driver J, Davis G, Ricciardelli P, Kidd P, Maxwell E, Baron-Cohen S. Gaze perception triggers reflexive visuospatial orienting. Vis cogn. 1999;6: 509–540. doi:10.1080/135062899394920

8. Langton SRH, Bruce V. Reflexive visual orienting in response to the social attention of others. Visual Cognition. 1999;6: 541–567. doi:10.1080/135062899394939

9. Langton SRH, Bruce V. You must see the point: Automatic processing of cues to the direction of social attention. J Exp Psychol Hum Percept Perform. 2000;26: 747–757. doi:10.1037/0096-1523.26.2.747

10. Friesen CK, Ristic J, Kingstone A. Attentional Effects of Counterpredictive Gaze and Arrow Cues. 2004;30: 319–329. doi:10.1037/0096-1523.30.2.319

11. Marciniak K, Dicke PW, Thier P. Monkeys head-gaze following is fast, precise and not fully suppressible. J Cogn Neurosci. 2008;20: 108–119. doi:10.1162/jocn.2008.20008

12. Perrett DI, Smith PAJ, Potter DD, Mistlin AJ, Head AS, Milner AD, et al. Visual Cells in the Temporal Cortex Sensitive to Face View and Gaze Direction. Proc R Soc B Biol Sci. 1985;223: 293–317. doi:10.1098/rspb.1985.0003

13. Hoffman EA, Haxby JV. Distinct representations of eye gaze and identity in the distributed human neural system for face perception. Nat Neurosci. 2000;3: 80–84. doi:10.1038/71152

14. Heywood CA, Cowey A. The role of the "face-cell" area in the discrimination and recognition of faces by monkeys. Philos Trans R Soc Lond B Biol Sci. 1992;335: 31–37; discussion 37-38. doi:10.1098/rstb.1992.0004

15. Akiyama T, Kato M, Muramatsu T, Saito F, Umeda S, Kashima H. Gaze but not arrows: A dissociative impairment after right superior temporal gyrus damage. Neuropsychologia. 2006;44: 1804–1810. doi:10.1016/j.neuropsychologia.2006.03.007

16. Kingstone A, Friesen CK, Gazzaniga MS. Reflexive joint attention depends on lateralized cortical connections. Psychol Sci. 2000;11: 159–166. doi:10.1111/1467-9280.00232

17. Nummenmaa L, Calder AJ. Neural mechanisms of social attention. Trends Cogn Sci. 2009;13: 135–143. doi:10.1016/j.tics.2008.12.006

18. Materna S, Dicke PW, Thier P. Dissociable Roles of the Superior Temporal Sulcus and the Intraparietal Sulcus in Joint Attention: A Functional Magnetic Resonance Imaging Study. J Cogn Neurosci. 2008;20: 108–119. doi:10.1098/rspb.2015.1020

19. Materna S, Dicke PW, Thier P. The posterior superior temporal sulcus is involved in social communication not specific for the eyes. Neuropsychologia. 2008;46: 2759–2765. doi:10.1016/j.neuropsychologia.2008.05.016

20. Laube I, Kamphuis S, Dicke PW, Thier P. Cortical processing of head- and eye-gaze cues guiding joint social attention. Neuroimage. 2011;54: 1643–1653. doi:10.1016/j.neuroimage.2010.08.074

21. Marquardt K, Ramezanpour H, Dicke PW, Thier P. Following Eye Gaze Activates a Patch in the Posterior Temporal Cortex That Is Not Part of the Human "Face Patch" System. eNeuro. 2017;4: 1–10. doi:10.1523/ENEURO.0317-16.2017

22. Kraemer PM, Görner M, Ramezanpour H, Dicke PW, Thier P. Frontal, Parietal, and Temporal Brain Areas Are Differentially Activated When Disambiguating Potential Objects of Joint Attention. eNeuro. 2020;7. doi:10.1523/ENEURO.0437-19.2020

23. Kamphuis S, Dicke PW, Thier P. Neuronal substrates of gaze following in monkeys. Eur J Neurosci. 2009;29: 1732–1738. doi:10.1111/j.1460-9568.2009.06730.x

24. Marciniak K, Atabaki A, Dicke PW, Thier P. Disparate substrates for head gaze following and face perception in the monkey superior temporal sulcus. Elife. 2014;3: 1–18. doi:10.7554/eLife.03222

25. Ramezanpour H, Thier P. Decoding of the other's focus of attention by a temporal cortex module. PNAS. 2020;117: 2663–2670. doi:10.1073/pnas.1911269117

26. Kanwisher N, McDermott J, Chun MM. The fusiform face area: a module in human extrastriate cortex specialized for face perception. J Neurosci. 1997;17: 4302–11. doi:10.1098/Rstb.2006.1934

27. Tsao DY, Moeller S, Freiwald WA. Comparing face patch systems in macaques and humans. Proc Natl Acad Sci. 2008;105: 19514–19519. doi:10.1073/pnas.0809662105

28. Stemmann H, Freiwald WA. Attentive Motion Discrimination Recruits an Area in Inferotemporal Cortex. J Neurosci. 2016;36: 11918–11928. doi:10.1523/JNEUROSCI.1888-16.2016

29. Huk AC, Dougherty RF, Heeger DJ. Retinotopy and Functional Subdivision of Human Areas MT and MST. J Neurosci. 2002;22: 7195–7205. doi:10.1523/JNEUROSCI.22-16-07195.2002

30. Kolster H, Peeters R, Orban GA. The Retinotopic Organization of the Human Middle Temporal Area MT/V5 and Its Cortical Neighbors. J Neurosci. 2010;30: 9801–9820. doi:10.1523/JNEUROSCI.2069-10.2010

31. Neurosynth. [cited 14 May 2022]. Available: https://neurosynth.org/

32. Born RT, Bradley DC. STRUCTURE AND FUNCTION OF VISUAL AREA MT. Annu Rev Neurosci. 2005;28: 157–189. doi:10.1146/annurev.neuro.26.041002.131052

33. Bunjes F, Gukelberger J. open source measurement system nrec. 2022. Available: https://nrec.neurologie.uni-tuebingen.de/nrec/

34. Esteban O, Markiewicz CJ, Blair RW, Moodie CA, Isik AI, Erramuzpe A, et al. fMRIPrep: a robust preprocessing pipeline for functional MRI. Nat Methods. 2019;16: 111–116. doi:10.1038/s41592-018-0235-4

35. Esteban O, Markiewicz CJ, Goncalves M, Provins C, Kent JD, DuPre E, et al. fMRIPrep: a robust preprocessing pipeline for functional MRI. Zenodo; 2022. doi:10.5281/zenodo.6928849

36. Gorgolewski K, Burns C, Madison C, Clark D, Halchenko Y, Waskom M, et al. Nipype: A Flexible, Lightweight and Extensible Neuroimaging Data Processing Framework in Python. Frontiers in Neuroinformatics. 2011;5. Available: https://www.frontiersin.org/articles/10.3389/fninf.2011.00013

37. Tustison NJ, Avants BB, Cook PA, Zheng Y, Egan A, Yushkevich PA, et al. N4ITK: Improved N3 Bias Correction. IEEE Transactions on Medical Imaging. 2010;29: 1310–1320. doi:10.1109/TMI.2010.2046908

38. Avants BB, Epstein CL, Grossman M, Gee JC. Symmetric diffeomorphic image registration with cross-correlation: Evaluating automated labeling of elderly and neurodegenerative brain. Medical Image Analysis. 2008;12: 26–41. doi:10.1016/j.media.2007.06.004

39. Zhang Y, Brady M, Smith S. Segmentation of brain MR images through a hidden Markov random field model and the expectation-maximization algorithm. IEEE Transactions on Medical Imaging. 2001;20: 45–57. doi:10.1109/42.906424

40. Dale AM, Fischl B, Sereno MI. Cortical Surface-Based Analysis: I. Segmentation and Surface Reconstruction. NeuroImage. 1999;9: 179–194. doi:10.1006/nimg.1998.0395

41. Klein A, Ghosh SS, Bao FS, Giard J, Häme Y, Stavsky E, et al. Mindboggling morphometry of human brains. PLOS Computational Biology. 2017;13: e1005350. doi:10.1371/journal.pcbi.1005350

42. Fonov V, Evans A, McKinstry R, Almli C, Collins D. Unbiased nonlinear average age-appropriate brain templates from birth to adulthood. NeuroImage. 2009;47: S102. doi:10.1016/S1053-8119(09)70884-5

43. Epidewarp. Available: https://www.nmr.mgh.harvard.edu/~greve/fbirn/b0/epidewarp.fsl

44. Glasser MF, Sotiropoulos SN, Wilson JA, Coalson TS, Fischl B, Andersson JL, et al. The minimal preprocessing pipelines for the Human Connectome Project. NeuroImage. 2013;80: 105–124. doi:10.1016/j.neuroimage.2013.04.127

45. Greve DN, Fischl B. Accurate and robust brain image alignment using boundary-based registration. NeuroImage. 2009;48: 63–72. doi:10.1016/j.neuroimage.2009.06.060

46. Jenkinson M, Bannister P, Brady M, Smith S. Improved Optimization for the Robust and Accurate Linear Registration and Motion Correction of Brain Images. NeuroImage. 2002;17: 825–841. doi:10.1006/nimg.2002.1132

47. Cox RW, Hyde JS. Software tools for analysis and visualization of fMRI data. NMR in Biomedicine. 1997;10: 171–178. doi:10.1002/(SICI)1099-1492(199706/08)10:4/5<171::AID-NBM453>3.0.CO;2-L

48. Power JD, Mitra A, Laumann TO, Snyder AZ, Schlaggar BL, Petersen SE. Methods to detect, characterize, and remove motion artifact in resting state fMRI. NeuroImage. 2014;84: 320–341. doi:10.1016/j.neuroimage.2013.08.048

49. Behzadi Y, Restom K, Liau J, Liu TT. A component based noise correction method (CompCor) for BOLD and perfusion based fMRI. NeuroImage. 2007;37: 90–101. doi:10.1016/j.neuroimage.2007.04.042

50. Satterthwaite TD, Elliott MA, Gerraty RT, Ruparel K, Loughead J, Calkins ME, et al. An improved framework for confound regression and filtering for control of motion artifact in the preprocessing of resting-state functional connectivity data. NeuroImage. 2013;64: 240–256. doi:10.1016/j.neuroimage.2012.08.052

51. Lanczos C. Evaluation of Noisy Data. Journal of the Society for Industrial and Applied Mathematics Series B Numerical Analysis. 1964;1: 76–85. doi:10.1137/0701007

52. Nilearn: Statistics for NeuroImaging in Python. [cited 14 May 2022]. Available: https://nilearn.github.io/index.html

53. Bolker B. GLMM FAQ. Available: http://bbolker.github.io/mixedmodels-misc/glmmFAQ.html

54. R Core Team. R: A Language and Environment for Statistical Computing. Vienna, Austria: R Foundation for Statistical Computing; 2021. Available: https://www.R-project.org/

55. Bürkner P-C. brms: An R Package for Bayesian Multilevel Models Using Stan. Journal of Statistical Software. 2017;80: 1–28. doi:10.18637/jss.v080.i01

56. Faulkenberry TJ. Savage-Dickey Density Ratio for computing Bayes Factors. In: The Book of Statistical Proofs [Internet]. 26 Aug 2020 [cited 14 May 2022]. Available: https://statproofbook.github.io/P/bf-sddr.html

57. Wetzels R, van Ravenzwaaij D, Wagenmakersq E-J. Bayesian Analysis. The Encyclopedia of Clinical Psychology. John Wiley & Sons, Ltd; 2015. pp. 1–11. Available: https://onlinelibrary.wiley.com/doi/abs/10.1002/9781118625392.wbecp453

58. Hollander G de, Knapen T. nideconv. Vrije Universiteit and the Spinoza Centre for Neuroimaging; 2017. Available: https://nideconv.readthedocs.io/en/latest/

59. Morey RD, Rouder JN, Jamil T, Urbanek S, Forner K, Ly A. BayesFactor. 2022. Available: https://richarddmorey.github.io/BayesFactor/

Acknowledgements

We thank Dr. Friedemann Bunjes for his invaluable technical assistance.

Author contributions

Marius Görner: Research design, data collection, analysis, and writing the manuscript. Peter Dicke: Data collection. Peter Thier: Research design and writing the manuscript.

Supplementary material

Model specification

The following table shows the *R* code in *brms* syntax for the models and the priors.

	Formula	Priors
Q1/2	$\beta \sim x + (x \mid\mid \text{run})$, family=gaussian(link="identity"), x = {condition, hemisphere}	normal(0, 5), class='Intercept' normal(0, 1), class='b', coef={'conditionGaze', hemisphereRH} normal(.5, .5), class='sd', coef='Intercept', group='run' normal(.3, .5), class='sd', coef='conditionGaze', group='run' lognormal(.5, .5), class='sigma'
Q1/2	$\beta \sim x + (x \mid\mid \text{participant/run})$, family=gaussian(link="identity"), x = {condition, hemisphere}	normal(0, 5), class='Intercept' normal(0, 1), class='b', coef={'conditionGaze', hemisphereRH} normal(.8, .5), class='sd', coef='Intercept', group='participant' normal(1, .5), class='sd', coef={'conditionGaze', hemisphereRH}, group='participant' normal(.8, .5), class='sd', coef='Intercept', group='participant:run' normal(.2, .5), class='sd', coef={'conditionGaze', hemisphereRH}, group='participant:run' lognormal(.5, .5), class='sigma'
Q3/4	$r \mid \text{trunc(lb=-1, ub=1)} \sim x$, family='gaussian', x = {lateralization, condition}	normal(0, 1), class='Intercept' normal(0, 2), class='b' lognormal(0, .5), class='sigma'
Q3/4	$r \mid \text{trunc(lb=-1, ub=1)} \sim x + (x \mid\mid \text{participant})$, family='gaussian', x = {lateralization, condition}	normal(0, 1), class='Intercept' normal(0, 2), class='b') normal(1, .5), class='sd', coef='Intercept', group='participant') normal(1, .5), class='sd', coef={'predicted_corrlow', 'consame'} group='participant') lognormal(0, .5), class='sigma'